
StableTTA: Training-Free Test-Time Adaptation that Improves Model Accuracy on ImageNet1K to 96%

Zheng Li

Department of Computer Science
New York Institute of Technology
New York, NY 10023
zli66@nyit.edu

Jerry Cheng

Department of Computer Science
New York Institute of Technology
New York, NY 10023
jcheng18@nyit.edu

Huanying Helen Gu

Department of Computer Science
New York Institute of Technology
New York, NY 10023
hgu03@nyit.edu

Abstract

Ensemble methods are widely used to improve predictive performance, but their effectiveness often comes at the cost of increased memory usage and computational complexity. In this paper, we identify a conflict in aggregation strategies that negatively impacts prediction stability. We propose StableTTA, a training-free method to improve aggregation stability and efficiency. Empirical results on ImageNet-1K show gains of 10.93–32.82% in top-1 accuracy, with 33 models achieving over 95% accuracy and several surpassing 96%. Notably, StableTTA allows lightweight architectures to outperform ViT by 11.75% in top-1 accuracy while using less than 5% of parameters and reducing computational cost by approximately 89.1% (in GFLOPs), enabling high-accuracy inference on resource-constrained devices. Code is available at: <https://github.com/LizhengMathAi/StableTTA>, including a 3-minute reproduction demo.

1 Introduction

Ensemble methods have long been proposed to improve the predictive quality of machine learning models [6]. By aggregating diverse predictions, they typically yield more accurate and robust outputs [6, 1]. These methods are usually training-free, meaning they do not require additional model training or extensive tuning of training recipes [1]. As a result, they are widely adopted by non-professional users seeking straightforward performance improvements. However, despite their simplicity, ensemble methods are rarely used in highly challenging, industrial-scale applications. Instead, researchers tend to focus on designing new model architectures, as these approaches often lead to better performance, fewer parameters, and lower computational costs during inference [4].

A key limitation of ensemble methods lies in their reliance on multiple models acting as “experts” to generate predictions for aggregation. This design leads to a linear increase in both memory usage and computational cost, as each additional model contributes to the total resource demand. In practice, using 10 models may result in less than a 3% improvement in accuracy, while increasing memory and inference cost by nearly 10×. Test-time augmentation (TTA) has been explored as a way to mitigate this trade-off by using a single model with multiple augmented inputs. However, this approach still scales linearly in computational cost with respect to the number of augmentations [7, 10] and does not fundamentally resolve the efficiency issue.

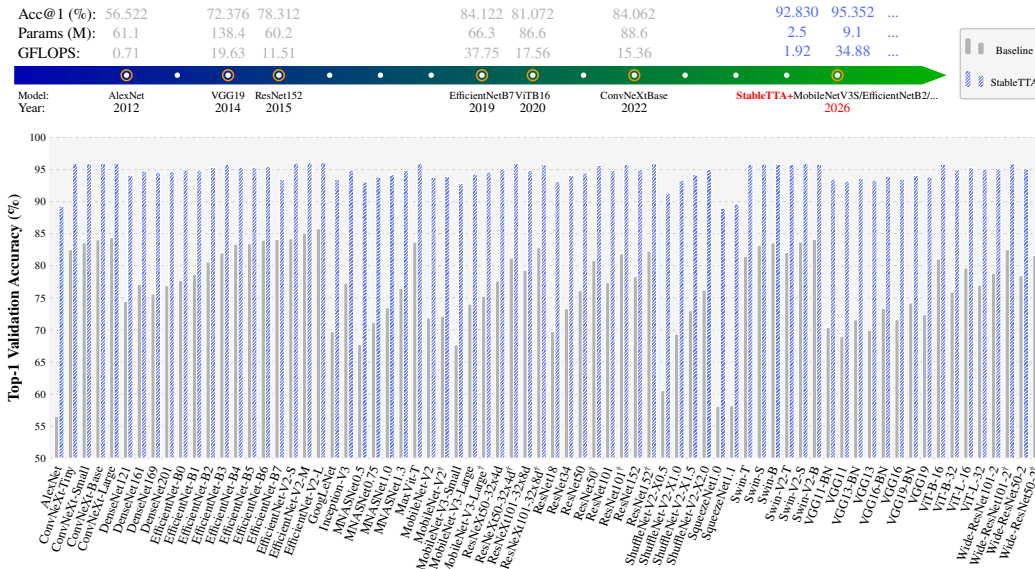


Figure 1: **Top: Milestone comparison.** We show that StableTTA+MobileNetV3 significantly outperforms the base ViT in terms of accuracy (+11.75% top-1), memory usage (-97% parameters), and computational cost (-89.1% GFLOPs). **Bottom: General comparison.** StableTTA improves baseline models by 11-33% in top-1 accuracy, with 34 models achieving more than 95% accuracy. The proposed method yields consistent and significant improvements across all evaluated models.

In this work, we identify and investigate an inherent conflict between different aggregation strategies. Based on this observation, we propose Training-Free Test-Time Adaptation (StableTTA), a hybrid method that combines image preprocessing with logit post-processing. Remarkably, this approach significantly improves the performance of popular vision models. Our experiments show gains of 10.93–32.82% in top-1 accuracy on the ImageNet-1K classification task. After applying StableTTA, 33 models achieve over 95% accuracy, and 4 models surpass 96%.

Historically, improvements in vision models on ImageNet-1K [3] have been incremental, typically yielding only 1–2% gains in top-1 accuracy per advancement [13, 28, 7, 31, 4], with accuracies above 90% [4, 17] requiring additional training data such as ImageNet-21K [25] and JFT-300M [20]. In contrast, without extra data, our method enables nearly all commonly used models to exceed 90% accuracy, with most surpassing 95%. More importantly, StableTTA addresses the core weakness of traditional ensemble methods by significantly improving memory efficiency and reducing computational cost. This makes it particularly suitable for mobile and resource-constrained environments. For example, our experiments show that a lightweight model such as MobileNetV3, when enhanced with StableTTA, significantly outperforms the Vision Transformer, achieving +11.75% higher top-1 accuracy while reducing memory usage by 97% and computational cost by 89.1% (measured in GFLOPs). These results demonstrate that StableTTA enables high-accuracy inference even on low-resource devices, outperforming larger models without requiring additional training.

2 Related Work

For image classification, model averaging is a widely used ensemble strategy to improve generalization performance [6]. As introduced by Breiman [1], outputs of multiple independently trained models are typically aggregated by majority voting on predictions or by averaging predicted probabilities. Generally, model averaging is not preferable to training a stronger, well-optimized single model [7]. Although it can provide modest performance gains, these improvements are often marginal relative to the substantial increase in resource requirements [7, 31]. Specifically, the total number of model parameters/FLOPs equals the sum of each model’s parameters/FLOPs.

Test-time augmentation (TTA) offers a partial alternative that avoids the need for multiple models. TTA applies a set of transformations to the input image (e.g., flipping, cropping) and feeds the augmented images into the same model to obtain multiple logits for averaging [13, 7]. This approach preserves the model size. However, it still increases the inference-time computation cost. For instance, ResNet [7] and DenseNet [10] employ 10-crop evaluation during validation. This increased the total FLOPs ten times. Despite these efforts, TTA typically yields only a modest improvement of no more than 2% in top-1 accuracy. [27, 12, 14].

Although TTA has been widely studied, only a few works gain attention in top-tier research, mainly because its key limitation “**the significant increase in inference computation**” remains unsolved.

3 Background

For a better understanding of the most commonly used ensemble methods, consider a C -class classification task. Let the logits \mathbf{z} denote the output vector of a model f with parameters θ for input \mathbf{x} :

$$\mathbf{z} = f(\mathbf{x}; \theta) \in \mathbb{R}^C.$$

After applying the softmax function, we obtain the probability distribution $\mathbf{p}_\theta(y | \mathbf{x})$ over the C classes:

$$\mathbf{p}_\theta(y = k | \mathbf{x}) = \frac{\exp(\mathbf{z}_k)}{\sum_{j=1}^C \exp(\mathbf{z}_j)}, \quad k = 1, \dots, C.$$

The predicted class is given by

$$\hat{y} = \arg \max_k \mathbf{z}_k = \arg \max_k \mathbf{p}_\theta(y = k | \mathbf{x}).$$

Majority voting, probability averaging, and logit averaging are commonly used aggregation strategies for ensemble methods, also known as hard voting, soft voting, and logit averaging, respectively [6, 22]. Consider an ensemble of N experts, the formal mathematical formulations are given as follows:

- Hard Voting (Fig. 2(b), orange blocks): Each model casts a vote for a class, and the class receiving the majority of votes is selected.

$$\text{(Hard Voting)} \quad \hat{y}_{\text{hard}} = \arg \max_k \sum_{i=1}^N \mathbb{1}_{\hat{y}^{(i)}=k}$$

- Soft Voting (Fig. 2(b), cyan blocks): The predicted class probabilities are averaged, and the class with the highest mean probability is selected.

$$\text{(Soft Voting)} \quad \hat{y}_{\text{soft}} = \arg \max_k \frac{1}{N} \sum_{i=1}^N \mathbf{p}^{(i)}(y = k | \mathbf{x})$$

- Logit Averaging (Fig. 2(b), light blue blocks): The logits are averaged across models, and the class with the highest mean logit is selected.

$$\text{(Logit Averaging)} \quad \hat{y}_{\text{logit}} = \arg \max_k \frac{1}{N} \sum_{i=1}^N \mathbf{z}_k^{(i)}$$

Limitations Fig. 2(a) illustrates the pipelines of model averaging and test-time augmentation (TTA) introduced in Section 2. Model averaging requires storing multiple models, and its inference-time computational cost is the sum of the costs of all models. In contrast, TTA uses a single model but increases the inference-time computational complexity by N (typically ranging from 5 to 64).

Conflict In ensemble methods, different aggregation strategies may conflict with one another. Fig. 2(b) illustrates such an example: given three logit vectors $(\mathbf{z}^{(1)}, \mathbf{z}^{(2)}, \mathbf{z}^{(3)})$, the predictions obtained from hard voting $\hat{y}_{\text{hard}} = 3$, soft voting $\hat{y}_{\text{soft}} = 2$, and logit averaging $\hat{y}_{\text{logit}} = 1$ are inconsistent. This discrepancy arises because both the softmax and indicator functions are nonlinear, leading to inconsistencies across aggregation strategies. This mismatch is a key factor contributing to the modest improvements typically observed in classification accuracy with ensemble methods.

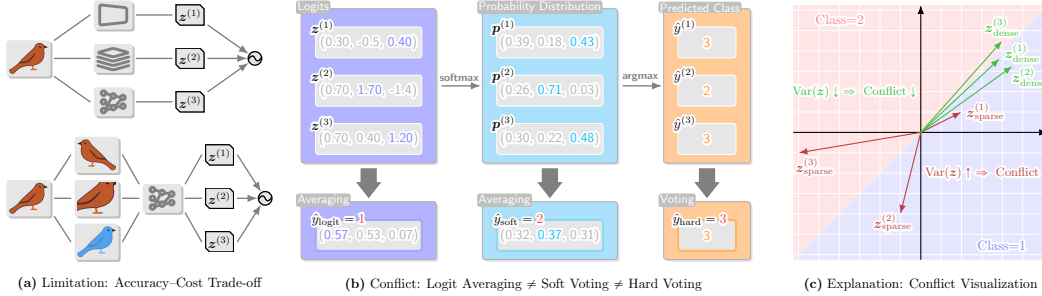


Figure 2: **Limitations of Ensemble Methods and Conflicts in Aggregation Strategies.** (a) **Limitations:** Illustration of model averaging and test-time augmentation (TTA) in image classification. Both methods significantly increase inference-time computational cost while providing only marginal improvements in accuracy. (b) **Conflict:** Given branch logits $\{z^{(i)} \mid i = 1, 2, 3\}$, probabilities $p^{(i)} = \text{softmax}(z^{(i)})$, and predictions $\hat{y}^{(i)} = \text{argmax } p^{(i)}$, different aggregation strategies can produce inconsistent results. In this example, logit averaging predicts class $\hat{y}_{\text{logit}} = 1$, soft voting predicts class $\hat{y}_{\text{soft}} = 2$, and hard voting predicts class $\hat{y}_{\text{hard}} = 3$. (c) **Explanation:** When the logits $(z^{(1)}, z^{(2)}, \dots)$ are sparsely distributed in space, the conflict $\hat{y}_{\text{logit}} \neq \hat{y}_{\text{soft}} \neq \hat{y}_{\text{hard}}$ is more likely to occur due to the nonlinearity and non-bijective nature of the softmax function. In contrast, when the logits are more densely clustered, such conflicts are less likely.

Interpretation of the Conflict As shown in Fig. 2(c), these conflicts arise from the distribution of logits in the feature space. When the logits $\{z^{(1)}, z^{(2)}, \dots\}$ are sparsely distributed, the nonlinearity and non-bijective nature of the softmax and indicator functions can amplify their differences.

In contrast, when the logits are more densely clustered, different aggregation strategies are more likely to yield consistent predictions. We provide both theoretical and empirical evidence to support this observation. In Appendix A, we further validate this phenomenon using Monte Carlo simulation (see Fig. 5), which show that as the variance $\text{Var}(z)$ increases, the probability of prediction conflicts also increases. The empirical results are well fitted by our derived relationship between $P(\hat{y}_{\text{logit}} \neq \hat{y}_{\text{hard}})$ and $\text{Var}(z)$. In summary, lower variance leads to fewer conflicts.

This observation inspires us to reformulate the test-time augmentation method and to design a logit-processing method to achieve more stable prediction aggregation.

4 Method

In this section, we aim to reduce $\text{Var}(z)$ through two approaches: (1) redesigning data augmentation strategies for TTA, and (2) introducing logit processing to further minimize logit variance.

4.1 Data Augmentation Principles for StableTTA

Since neural network layers are continuous and differentiable, most neural networks satisfy the Hölder condition [35]:

$$\|z - z'\| = \|f(x; \theta) - f(x'; \theta)\| \leq c \cdot \|x - x'\|^d$$

where c and d are constants. This inequality indicates that the distance $\|z - z'\|$ between logits is determined by the distance $\|x - x'\|$ between inputs.

Now, consider a sequence of data augmentations $\{\psi_1, \psi_2, \dots\}$ and the corresponding logit vector $z^{(i)} := f(\psi_i(x); \theta)$. By applying the Hölder condition, we obtain:

$$\|z^{(i)} - z^{(j)}\| = \|f(\psi_i(x); \theta) - f(\psi_j(x); \theta)\| \leq c \|\psi_i(x) - \psi_j(x)\|^d. \quad (1)$$

Furthermore, when $d \in (0, 1]$, we have:

$$\text{Var}(z) \leq 2^{d-1} c^2 \text{Var}(\psi(x)).$$

To facilitate understanding Eq. (1), in Appendix B, we provide Fig. 6 for visualization, along with empirical results as supporting evidence.

Now, reviewing the conflict discussed in Section 3, we draw the following conclusions:

- Common augmentation techniques such as horizontal flipping and random cropping are not necessary in TTA, as the model is not sensitive to them. Pre-trained models already account for these transformations; thus, the logit vectors are typically identical after such augmentations.
- Common augmentation techniques such as translation, rotation, and affine transformations [2] should be avoided in TTA, as they can induce an excessively large increase in $\text{Var} \|\psi(\mathbf{x})\|$.
- Although random erasing yields relatively small values of $\text{Var}(\psi(\mathbf{x}))$, it provides limited diversity among augmented samples and is therefore excluded.

Under these considerations, mixup [39] and CutMix [37] emerge as promising candidates. However, both require further modification to reduce $\text{Var}(\psi(\mathbf{x}))$:

- **Mixup:** Instead of combining the input with a random image, we perform a weighted combination with a fixed image, which is randomly sampled and kept unchanged thereafter.
- **CutMix:** The covering region is typically sampled from a Beta distribution to encourage diversity during training. In contrast, we fix the window size to one-quarter of the image to reduce $\text{Var}(\psi(\mathbf{x}))$.
- **Random Choice:** Standard pipelines often compose multiple augmentations sequentially. Here, we randomly choose one of them in each inference step to better control $\text{Var}(\psi(\mathbf{x}))$.

4.2 Logits Processing for StableTTA

Referring to the example in Fig. 2(b), a class that is not significant in individual predictions should not emerge as the final prediction solely because it attains the highest averaged logit. To address this issue, we propose Non-Significant Suppression (NSS) to averaging:

$$\text{NSS}(\mathbf{z}, K) := \mathbf{z} \odot \mathbf{1}_{\text{TopK}(\mathbf{z}, K)} + \min(\mathbf{z}) \cdot (\mathbf{1} - \mathbf{1}_{\text{TopK}(\mathbf{z}, K)}), \quad K = 1, \dots, C \quad (2)$$

where, $\mathbf{1}$ is the all-ones vector, $\mathbf{1}_{\text{TopK}(\mathbf{z}, K)} \in \{0, 1\}^d$ is the indicator vector of the Top- K indices (equal to 1 for indices in the Top- K set and 0 otherwise), and \odot denotes element-wise multiplication. In this work, we apply NSS to logits averaging as a processing method and prove that it reduces $\text{Var}(\mathbf{z})$.

From the definition of NSS, we have:

$$\text{NSS}(\mathbf{z}, K)_i = \begin{cases} z_i, & i \in \text{TopK}(\mathbf{z}, K), \\ \min(\mathbf{z}), & i \notin \text{TopK}(\mathbf{z}, K), \end{cases}$$

and

$$\frac{\partial}{\partial z_j} \text{NSS}(\mathbf{z}, K)_i = \begin{cases} 1, & \text{if } i \in \text{TopK}(\mathbf{z}, K) \text{ and } i = j, \\ 0, & \text{if } i \in \text{TopK}(\mathbf{z}, K) \text{ and } i \neq j, \\ 1, & \text{if } i \notin \text{TopK}(\mathbf{z}, K) \text{ and } j = \arg \min \mathbf{z}, \\ 0, & \text{if } i \notin \text{TopK}(\mathbf{z}, K) \text{ and } j \neq \arg \min \mathbf{z}. \end{cases}$$

Hence, almost everywhere,

$$\|\nabla \text{NSS}(\mathbf{z}, K)_i\|^2 = \sum_{j=1}^C \left(\frac{\partial}{\partial z_j} \text{NSS}(\mathbf{z}, K)_i \right)^2 = 1.$$

In particular,

$$\|\nabla \text{NSS}(\mathbf{z}, K)_i\|^2 \leq 1.$$

Then if $\mathbf{z} \sim \mathcal{N}(\boldsymbol{\mu}, \sigma^2 \mathbf{I})$. Gaussian Poincaré inequality gives

$$\text{Var}(\text{NSS}(\mathbf{z}, K)_i) \leq \mathbb{E} \left[\sigma^2 \|\nabla \text{NSS}(\mathbf{z}, K)_i\|^2 \right] \leq \sigma^2 = \text{Var}(z_i).$$

This implies that NSS reduces the variance of each logit z_i , thereby further avoiding the conflict described in Section 3. In Section 5.3, we discuss the impact of NSS and explore the parameter K , which represents the number of candidates; for additional details, see Appendix D.

4.3 Effectiveness of Augmentation and Logit Processing in StableTTA

We summarize the overall formulation of StableTTA as follows:

$$z \leftarrow \frac{1}{N} \sum_{i=1}^N \text{NSS}(f(\psi^{(i)}(\mathbf{x}); \theta), K), \quad \psi^{(i)} \in \{\psi_{\text{mixup}}^*, \psi_{\text{CutMix}}^*\},$$

where ψ_{mixup}^* and ψ_{CutMix}^* denote our proposed data augmentation strategies.

Our proposed data augmentation strategies consistently yield an additional 4–10% improvement in top-1 accuracy compared to standard mixup and CutMix. These gains also surpass other standard augmentation techniques, such as flipping and cropping. Detailed ablation results are provided in Section 5.2 and Appendix C.

Our logit processing method can only be applied when the required stability data augmentations are used (such as the proposed specialized mixup and CutMix). Nevertheless, as demonstrated in the sensitivity analysis in Section 3, it provides an additional 5–12% improvement in top-1 accuracy on already strong baseline models. Detailed experimental results are provided in Section 5.3 and Appendix D. It is important to note that

$$\text{NSS}(z, C) = z \odot \mathbf{1} + \min(z) \cdot (\mathbf{1} - \mathbf{1}) = z,$$

which implies that when $K = C$, StableTTA is downgraded to enhance model performance using only our data augmentation strategies, without applying logit processing.

5 Experiments

We evaluate the model-boosting capability of StableTTA in terms of accuracy, memory usage, and computational cost. To provide a comprehensive understanding, we first present a full comparison across a wide range of popular models on ImageNet-1K. We then provide visualizations demonstrating that StableTTA enables lightweight architectures to outperform larger models in terms of top-1 accuracy, memory efficiency, and computational cost. Finally, we present ablation studies and sensitivity analysis to further examine the effectiveness and robustness of our method.

Dataset. ImageNet-1K [3] is a highly challenging and widely used benchmark dataset, which we adopt for evaluation. It contains 1.28 million training images and 50,000 validation images across 1,000 categories. Over the past years, well-established models have typically achieved only incremental improvements of 1–2% in top-1 accuracy per advancement [13, 28, 7, 31, 4].

Models. All pretrained models used in our experiments are publicly available in torchvision [21], including official implementations, subsequent improvements, and recent training recipes that achieve state-of-the-art performance [23]. We denote these enhanced variants with “†” in this paper.

Evaluation. We directly evaluate model performance on a single NVIDIA RTX A6000 GPU. Unless otherwise specified, we use the number of experts $N = 32$, the number of candidates $K = 10$, and a batch size of 16 on the ImageNet-1K validation set. We compare four settings: (1) baseline models, (2) baseline with TTA using our recommend data augmentation strategy, and (3) baseline with StableTTA. Despite stochastic components, results are highly stable, with accuracy variation below 0.01. Both baseline and StableTTA use the same evaluation pipeline, including single-crop inference.

5.1 Main Results

We cite the corresponding architecture and training recipe for each pretrained model. Table 1 demonstrates that StableTTA yields substantial and consistent improvements in top-1 and top-5 accuracy across popular ImageNet-1K models, while also reporting parameter counts and computational cost.

Across all model families, StableTTA provides large accuracy gains, typically ranging from 10.93% to over 32.82% in top-1 accuracy. Notably, even early architectures such as AlexNet and lightweight models such as MobileNet and ShuffleNet achieve performance comparable to or exceeding that of modern large-scale models. Furthermore, a significant number of models surpass the 95% top-1

accuracy threshold, with several exceeding 96%, indicating a strong saturation of performance across diverse architectures.

Importantly, Fig. 3 shows that these improvements are achieved without increasing model parameters or inference complexity in the serial setting, highlighting the efficiency of StableTTA. In the parallel setting, StableTTA increases inference cost by a factor of N ; however, when applied to lightweight architectures, it remains significantly more economical than using large models. This demonstrates a favorable trade-off between accuracy, memory usage, and computational cost. These results suggest that StableTTA effectively bridges the gap between lightweight and high-performance models, enabling practical deployment in resource-constrained environments.

Table 1: Comparison with popular ImageNet-1K classification benchmarks. We compare baseline performance with our proposed StableTTA, reporting model size, computational cost, and significant improvements in top-1 and top-5 validation accuracy.

Weight	Params	Peak GFLOPS	Baseline (%)		StableTTA (%)	
			Acc@1	Acc@5	Acc@1	Acc@5
AlexNet [13, 21]	61.1M	0.71	56.522	79.066	89.332	98.028
ConvNeXt_Tiny [17, 21]	28.6M	4.46	82.52	96.146	95.958	99.884
ConvNeXt_Small [17, 21]	50.2M	8.68	83.616	96.65	95.932	99.914
ConvNeXt_Base [17, 21]	88.6M	15.36	84.062	96.87	95.964	99.906
ConvNeXt_Large [17, 21]	197.8M	34.36	84.414	96.976	95.998	99.932
DenseNet121 [10, 21]	8.0M	2.83	74.434	91.972	94.160	99.370
DenseNet161 [10, 21]	28.7M	7.73	77.138	93.56	94.814	99.572
DenseNet169 [10, 21]	14.1M	3.36	75.6	92.806	94.600	99.510
DenseNet201 [10, 21]	20.0M	4.29	76.896	93.37	94.734	99.562
EfficientNet_B0 [31, 21]	5.3M	0.39	77.692	93.532	94.988	99.678
EfficientNet_B1 [31, 21]	7.8M	0.69	78.642	94.186	94.940	99.738
EfficientNet_B2 [31, 21]	9.1M	1.09	80.608	95.31	95.352	99.796
EfficientNet_B3 [31, 21]	12.2M	1.83	82.008	96.054	95.816	99.862
EfficientNet_B4 [31, 21]	19.3M	4.39	83.384	96.594	95.386	99.874
EfficientNet_B5 [31, 21]	30.4M	10.27	83.444	96.628	95.328	99.872
EfficientNet_B6 [31, 21]	43.0M	19.07	84.008	96.916	95.504	99.892
EfficientNet_B7 [31, 21]	66.3M	37.75	84.122	96.908	93.452	99.718
EfficientNet_V2_S [32, 21]	21.5M	8.37	84.228	96.878	96.046	99.926
EfficientNet_V2_M [32, 21]	54.1M	24.58	85.112	97.156	96.102	99.920
EfficientNet_V2_L [32, 21]	118.5M	56.08	85.808	97.788	96.164	99.892
GoogLeNet [29, 21]	6.6M	1.5	69.778	89.53	93.510	99.346
Inception_V3 [30, 21]	27.2M	5.71	77.294	93.45	94.906	99.734
MNASNet0_5 [33, 21]	2.2M	0.1	67.734	87.49	93.122	99.188
MNASNet0_75 [33, 21]	3.2M	0.21	71.18	90.496	93.868	99.484
MNASNet1_0 [33, 21]	4.4M	0.31	73.456	91.51	94.230	99.342
MNASNet1_3 [33, 21]	6.3M	0.53	76.506	93.522	94.876	99.728
MaxVit_T [34, 21]	30.9M	5.56	83.7	96.722	95.996	99.902
MobileNet_V2 [26, 21]	3.5M	0.3	71.878	90.286	93.784	99.262
MobileNet_V2 [†] [26, 23]	3.5M	0.3	72.154	90.822	93.922	99.516
MobileNet_V3_Small [9, 21]	2.5M	0.06	67.668	87.402	92.830	99.094
MobileNet_V3_Large [9, 21]	5.5M	0.22	74.042	91.34	94.350	99.364
MobileNet_V3_Large [†] [9, 23]	5.5M	0.22	75.274	92.566	94.648	99.656
ResNeXt50_32x4d [36, 21]	25.0M	4.23	77.618	93.698	95.126	99.680
ResNeXt50_32x4d [†] [36, 23]	25.0M	4.23	81.198	95.34	95.978	99.916
ResNeXt101_32x8d [36, 21]	88.8M	16.41	79.312	94.526	94.862	99.648
ResNeXt101_32x8d [†] [36, 23]	88.8M	16.41	82.834	96.228	95.764	99.874
ResNet18 [7, 21]	11.7M	1.81	69.758	89.078	93.176	99.194
ResNet34 [7, 21]	21.8M	3.66	73.314	91.42	94.092	99.406
ResNet50 [7, 21]	25.6M	4.09	76.13	92.862	94.518	99.496
ResNet50 [†] [7, 23]	25.6M	4.09	80.858	95.434	95.666	99.866
ResNet101 [7, 21]	44.5M	7.8	77.374	93.546	94.858	99.540

Continued on next page

Weight	Params	GFLOPS	Acc@1	Acc@5	Acc@1	Acc@5
ResNet101 [†] [7, 23]	44.5M	7.8	81.886	95.78	95.804	99.890
ResNet152 [7, 21]	60.2M	11.51	78.312	94.046	95.018	99.558
ResNet152 [†] [7, 23]	60.2M	11.51	82.284	96.002	95.942	99.890
ShuffleNet_V2_X0_5 [19, 21]	1.4M	0.04	60.552	81.746	91.372	98.724
ShuffleNet_V2_X1_0 [19, 21]	2.3M	0.14	69.362	88.316	93.380	99.342
ShuffleNet_V2_X1_5 [19, 21]	3.5M	0.3	72.996	91.086	94.238	99.580
ShuffleNet_V2_X2_0 [19, 21]	7.4M	0.58	76.23	93.006	94.996	99.716
SqueezeNet1_0 [11, 21]	1.2M	0.82	58.092	80.42	89.030	97.878
SqueezeNet1_1 [11, 21]	1.2M	0.35	58.178	80.624	89.642	98.020
Swin_T [15, 21]	28.3M	4.49	81.474	95.776	95.798	99.864
Swin_S [15, 21]	49.6M	8.74	83.196	96.36	95.894	99.914
Swin_B [15, 21]	87.8M	15.43	83.582	96.64	95.832	99.916
Swin_V2_T [16, 21]	28.4M	5.94	82.072	96.132	95.798	99.864
Swin_V2_S [16, 21]	49.7M	11.55	83.712	96.816	96.024	99.902
Swin_V2_B [16, 21]	87.9M	20.32	84.112	96.864	95.890	99.938
VGG11_BN [28, 21]	132.9M	7.61	70.37	89.81	93.542	99.124
VGG11 [28, 21]	132.9M	7.61	69.02	88.628	93.236	99.038
VGG13_BN [28, 21]	133.1M	11.31	71.586	90.374	93.666	99.190
VGG13 [28, 21]	133.0M	11.31	69.928	89.246	93.400	99.084
VGG16_BN [28, 21]	138.4M	15.47	73.36	91.516	93.978	98.242
VGG16 [28, 21]	138.4M	15.47	71.592	90.382	93.542	99.164
VGG19_BN [28, 21]	138.4M	19.63	74.218	91.842	94.122	99.266
VGG19 [28, 21]	138.4M	19.63	72.376	90.876	93.868	99.246
ViT_B_16 [4, 21]	86.6M	17.56	81.072	95.318	95.850	99.886
ViT_B_32 [4, 21]	88.2M	4.41	75.912	92.466	95.000	99.778
ViT_L_16 [4, 21]	304.3M	61.55	79.662	94.638	95.314	99.860
ViT_L_32 [4, 21]	306.5M	15.38	76.972	93.07	95.132	99.804
Wide_ResNet101_2 [38, 21]	126.9M	22.75	78.848	94.284	95.146	99.666
Wide_ResNet101_2 [†] [38, 23]	126.9M	22.75	82.51	96.02	95.914	99.898
Wide_ResNet50_2 [38, 21]	68.9M	11.4	78.468	94.086	95.168	99.654
Wide_ResNet50_2 [†] [38, 23]	68.9M	11.4	81.602	95.758	95.736	99.868

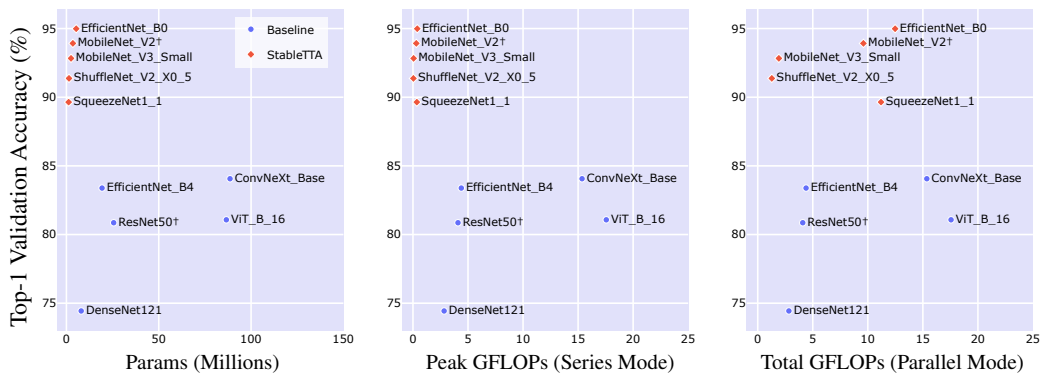


Figure 3: **Efficiency–Accuracy Trade-offs.** Comparison of baseline (blue) and StableTTA (red) across parameters (left), peak GFLOPs in series mode (middle), and total GFLOPs in parallel mode (right). Series mode processes images sequentially, while parallel mode processes augmented inputs simultaneously. StableTTA improves accuracy while maintaining favorable efficiency, enabling lightweight models to outperform larger ones.

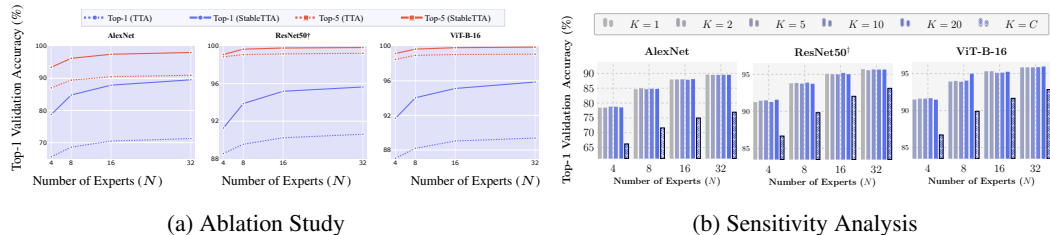


Figure 4: (a) TTA (with our augmentation) vs. StableTTA. (b) StableTTA is robust to K and mainly affected by N , but disabling logit processing ($K = C$) will significantly reduce top-1 accuracy.

5.2 Ablation Study

We compare standard test-time augmentation (TTA) using MixUp and CutMix with our proposed StableTTA. As shown in Fig. 4a, StableTTA consistently outperforms standard TTA across different models and numbers of experts (N), achieving higher top-1 and top-5 accuracy while maintaining stable performance gains as N increases.

We also observe a diminishing marginal effect as N increases, indicating that larger numbers of experts provide limited additional benefit. Therefore, we adopt $N = 32$ in Table 1 as a practical setting that balances performance and computational cost.

We do not consider additional TTA strategies such as flipping, cropping, or image translation, as their improvements are modest (typically less than 2%) [27, 12, 14]. More detailed ablation results are provided in Appendix C.

5.3 Sensitivity Analysis

We analyze the sensitivity of StableTTA to key hyperparameters, including the number of candidates K and the number of experts N . As shown in Fig. 4b, StableTTA demonstrates strong robustness to the choice of N , with performance remaining stable across a wide range of values. In contrast, the number of candidates N has only a marginal effect on top-1 accuracy, indicating that StableTTA does not rely heavily on large ensemble sizes.

Importantly, when logit processing is disabled ($K = C$), the performance drops significantly, highlighting its critical role in achieving accuracy gains. These results suggest that StableTTA provides stable and reliable improvements without requiring careful hyperparameter tuning. Additional sensitivity analysis results are provided in Appendix D.

5.4 Limitations and Future Work

The proposed method can be executed in either sequential or parallel modes. In sequential mode, it does not require additional computational resources beyond a single model, but it increases inference latency approximately in proportion to N due to aggregation. In contrast, parallel execution achieves inference time comparable to that of a single model with a single forward pass, at the cost of N times the computational resources. This trade-off motivates our evaluation in Fig. 3: we compare StableTTA applied to lightweight architectures against large models, rather than comparing StableTTA-enhanced large models to their original counterparts. Using lightweight models ensures that the increased computational cost and runtime introduced by StableTTA remain lower than those of a single large model.

For future work, we plan to extend StableTTA to other tasks, such as semantic segmentation [18] and object detection [24], and explore its integration with techniques such as model pruning [5] and knowledge distillation [8].

6 Conclusion

In this work, we reconstructed the efficiency–performance trade-off inherent in ensemble methods and observed a fundamental conflict in conventional aggregation strategies that limits prediction

stability. To address this issue, we introduced StableTTA, a simple yet effective training-free approach that combines image preprocessing with logit post-processing to improve the stability of aggregation.

Extensive experiments on ImageNet-1K demonstrate that StableTTA delivers substantial and consistent improvements across a wide range of models, boosting top-1 accuracy by 11–33% and enabling the majority of evaluated architectures to surpass 95% accuracy. Notably, our method allows lightweight models to outperform significantly larger architectures while drastically reducing memory footprint and computational cost. This highlights StableTTA’s potential as a practical solution for deploying high-accuracy vision systems in resource-constrained environments.

Overall, StableTTA challenges the conventional reliance on larger models and costly ensembles by showing that simple aggregation can unlock significant performance gains. We hope this work encourages further exploration of training-free adaptation methods that enhance both efficiency and robustness across a broader range of applications, such as semantic segmentation and object detection.

References

- [1] Leo Breiman. Bagging predictors. *Machine learning*, 24(2):123–140, 1996.
- [2] Ekin D Cubuk, Barret Zoph, Dandelion Mane, Vijay Vasudevan, and Quoc V Le. Autoaugment: Learning augmentation strategies from data. In *Proceedings of the IEEE/CVF conference on computer vision and pattern recognition*, pages 113–123, 2019.
- [3] Jia Deng, Wei Dong, Richard Socher, Li-Jia Li, Kai Li, and Li Fei-Fei. Imagenet: A large-scale hierarchical image database. In *2009 IEEE conference on computer vision and pattern recognition*, pages 248–255. Ieee, 2009.
- [4] Alexey Dosovitskiy, Lucas Beyer, Alexander Kolesnikov, Dirk Weissenborn, Xiaohua Zhai, Thomas Unterthiner, Mostafa Dehghani, Matthias Minderer, Georg Heigold, Sylvain Gelly, et al. An image is worth 16x16 words: Transformers for image recognition at scale. *arXiv preprint arXiv:2010.11929*, 2020.
- [5] Song Han, Jeff Pool, John Tran, and William Dally. Learning both weights and connections for efficient neural network. *Advances in neural information processing systems*, 28, 2015.
- [6] Trevor Hastie. *The elements of statistical learning: data mining, inference, and prediction*, 2009.
- [7] Kaiming He, Xiangyu Zhang, Shaoqing Ren, and Jian Sun. Deep residual learning for image recognition. In *Proceedings of the IEEE conference on computer vision and pattern recognition*, pages 770–778, 2016.
- [8] Geoffrey Hinton, Oriol Vinyals, and Jeff Dean. Distilling the knowledge in a neural network. *arXiv preprint arXiv:1503.02531*, 2015.
- [9] Andrew Howard, Mark Sandler, Grace Chu, Liang-Chieh Chen, Bo Chen, Mingxing Tan, Weijun Wang, Yukun Zhu, Ruoming Pang, Vijay Vasudevan, et al. Searching for mobilenetv3. In *Proceedings of the IEEE/CVF international conference on computer vision*, pages 1314–1324, 2019.
- [10] Gao Huang, Zhuang Liu, Laurens Van Der Maaten, and Kilian Q Weinberger. Densely connected convolutional networks. In *Proceedings of the IEEE conference on computer vision and pattern recognition*, pages 4700–4708, 2017.
- [11] Forrest N Iandola, Song Han, Matthew W Moskewicz, Khalid Ashraf, William J Dally, and Kurt Keutzer. Squeezenet: Alexnet-level accuracy with 50x fewer parameters and < 0.5 mb model size. *arXiv preprint arXiv:1602.07360*, 2016.
- [12] Ildoo Kim, Younghoon Kim, and Sungwoong Kim. Learning loss for test-time augmentation. *Advances in neural information processing systems*, 33:4163–4174, 2020.
- [13] Alex Krizhevsky, Ilya Sutskever, and Geoffrey E Hinton. Imagenet classification with deep convolutional neural networks. *Advances in neural information processing systems*, 25, 2012.

- [14] Zheng Li, Jerry Cheng, and Huanying Helen Gu. Losstransform: Reformulating the loss function for contrastive learning. *Information*, 16(12):1068, 2025.
- [15] Ze Liu, Yutong Lin, Yue Cao, Han Hu, Yixuan Wei, Zheng Zhang, Stephen Lin, and Baining Guo. Swin transformer: Hierarchical vision transformer using shifted windows. In *Proceedings of the IEEE/CVF international conference on computer vision*, pages 10012–10022, 2021.
- [16] Ze Liu, Han Hu, Yutong Lin, Zhuliang Yao, Zhenda Xie, Yixuan Wei, Jia Ning, Yue Cao, Zheng Zhang, Li Dong, et al. Swin transformer v2: Scaling up capacity and resolution. In *Proceedings of the IEEE/CVF conference on computer vision and pattern recognition*, pages 12009–12019, 2022.
- [17] Zhuang Liu, Hanzi Mao, Chao-Yuan Wu, Christoph Feichtenhofer, Trevor Darrell, and Saining Xie. A convnet for the 2020s. In *Proceedings of the IEEE/CVF conference on computer vision and pattern recognition*, pages 11976–11986, 2022.
- [18] Jonathan Long, Evan Shelhamer, and Trevor Darrell. Fully convolutional networks for semantic segmentation. In *Proceedings of the IEEE conference on computer vision and pattern recognition*, pages 3431–3440, 2015.
- [19] Ningning Ma, Xiangyu Zhang, Hai-Tao Zheng, and Jian Sun. Shufflenet v2: Practical guidelines for efficient cnn architecture design. In *Proceedings of the European conference on computer vision (ECCV)*, pages 116–131, 2018.
- [20] Dhruv Mahajan, Ross Girshick, Vignesh Ramanathan, Kaiming He, Manohar Paluri, Yixuan Li, Ashwin Bharambe, and Laurens Van Der Maaten. Exploring the limits of weakly supervised pretraining. In *Proceedings of the European conference on computer vision (ECCV)*, pages 181–196, 2018.
- [21] TorchVision maintainers and contributors. Torchvision: Pytorch’s computer vision library. <https://github.com/pytorch/vision>, 2016.
- [22] Fabian Pedregosa, Gaël Varoquaux, Alexandre Gramfort, Vincent Michel, Bertrand Thirion, Olivier Grisel, Mathieu Blondel, Peter Prettenhofer, Ron Weiss, Vincent Dubourg, et al. Scikit-learn: Machine learning in python. *the Journal of machine Learning research*, 12:2825–2830, 2011.
- [23] PyTorch Team. How to train state-of-the-art models using torchvision’s latest primitives. <https://pytorch.org/blog/how-to-train-state-of-the-art-models-using-torchvision-latest-primitives/>, 2021. Accessed: 2026-03-25.
- [24] Shaoqing Ren, Kaiming He, Ross Girshick, and Jian Sun. Faster r-cnn: Towards real-time object detection with region proposal networks. *Advances in neural information processing systems*, 28, 2015.
- [25] Tal Ridnik, Emanuel Ben-Baruch, Asaf Noy, and Lihi Zelnik-Manor. Imagenet-21k pretraining for the masses. *arXiv preprint arXiv:2104.10972*, 2021.
- [26] Mark Sandler, Andrew Howard, Menglong Zhu, Andrey Zhmoginov, and Liang-Chieh Chen. Mobilenetv2: Inverted residuals and linear bottlenecks. In *Proceedings of the IEEE conference on computer vision and pattern recognition*, pages 4510–4520, 2018.
- [27] Divya Shanmugam, Davis Blalock, Guha Balakrishnan, and John Gutttag. Better aggregation in test-time augmentation. In *Proceedings of the IEEE/CVF international conference on computer vision*, pages 1214–1223, 2021.
- [28] Karen Simonyan and Andrew Zisserman. Very deep convolutional networks for large-scale image recognition. *arXiv preprint arXiv:1409.1556*, 2014.
- [29] Christian Szegedy, Wei Liu, Yangqing Jia, Pierre Sermanet, Scott Reed, Dragomir Anguelov, Dumitru Erhan, Vincent Vanhoucke, and Andrew Rabinovich. Going deeper with convolutions. In *Proceedings of the IEEE conference on computer vision and pattern recognition*, pages 1–9, 2015.

- [30] Christian Szegedy, Vincent Vanhoucke, Sergey Ioffe, Jon Shlens, and Zbigniew Wojna. Rethinking the inception architecture for computer vision. In *Proceedings of the IEEE conference on computer vision and pattern recognition*, pages 2818–2826, 2016.
- [31] Mingxing Tan and Quoc Le. Efficientnet: Rethinking model scaling for convolutional neural networks. In *International conference on machine learning*, pages 6105–6114. PMLR, 2019.
- [32] Mingxing Tan and Quoc Le. Efficientnetv2: Smaller models and faster training. In *International conference on machine learning*, pages 10096–10106. PMLR, 2021.
- [33] Mingxing Tan, Bo Chen, Ruoming Pang, Vijay Vasudevan, Mark Sandler, Andrew Howard, and Quoc V Le. Mnasnet: Platform-aware neural architecture search for mobile. In *Proceedings of the IEEE/CVF conference on computer vision and pattern recognition*, pages 2820–2828, 2019.
- [34] Zhengzhong Tu, Hossein Talebi, Han Zhang, Feng Yang, Peyman Milanfar, Alan Bovik, and Yinxiao Li. Maxvit: Multi-axis vision transformer. In *European conference on computer vision*, pages 459–479. Springer, 2022.
- [35] Aladin Virmaux and Kevin Scaman. Lipschitz regularity of deep neural networks: analysis and efficient estimation. *Advances in neural information processing systems*, 31, 2018.
- [36] Saining Xie, Ross Girshick, Piotr Dollár, Zhuowen Tu, and Kaiming He. Aggregated residual transformations for deep neural networks. In *Proceedings of the IEEE conference on computer vision and pattern recognition*, pages 1492–1500, 2017.
- [37] Sangdoon Yun, Dongyoon Han, Seong Joon Oh, Sanghyuk Chun, Junsuk Choe, and Youngjoon Yoo. Cutmix: Regularization strategy to train strong classifiers with localizable features. In *Proceedings of the IEEE/CVF international conference on computer vision*, pages 6023–6032, 2019.
- [38] Sergey Zagoruyko and Nikos Komodakis. Wide residual networks. *arXiv preprint arXiv:1605.07146*, 2016.
- [39] Hongyi Zhang, Moustapha Cisse, Yann N Dauphin, and David Lopez-Paz. mixup: Beyond empirical risk minimization. In *International Conference on Learning Representations*, 2018.

A Monte Carlo Simulation

Consider the logit vector $\mathbf{z} \sim \mathcal{N}(\boldsymbol{\mu}, \sigma^2 \mathbf{I})$ in a binary classification task. Then,

$$\mathbb{E} \begin{pmatrix} z_1 - z_2 \\ \mathbb{1}_{z_1 > z_2} \end{pmatrix} = \begin{bmatrix} \boldsymbol{\mu}_1 - \boldsymbol{\mu}_2 \\ \Phi \left(\frac{\boldsymbol{\mu}_1 - \boldsymbol{\mu}_2}{\sqrt{2}\sigma} \right) \end{bmatrix}, \quad (3)$$

$$\text{Var} \begin{pmatrix} z_1 - z_2 \\ \mathbb{1}_{z_1 > z_2} \end{pmatrix} = \begin{bmatrix} 2\sigma^2 & \sqrt{2}\sigma\phi(a) \\ \sqrt{2}\sigma\phi(a) & \phi(a) - \phi^2(a) \end{bmatrix}, \quad (4)$$

where

$$a = \frac{\boldsymbol{\mu}_1 - \boldsymbol{\mu}_2}{\sqrt{2}\sigma}.$$

By the Central Limit Theorem, for large N , the sample averages satisfy

$$\begin{pmatrix} \frac{1}{N} \sum_{i=1}^N z_1^{(i)} - z_2^{(i)} \\ \frac{1}{N} \sum_{i=1}^N \mathbb{1}_{z_1^{(i)} > z_2^{(i)}} \end{pmatrix} \sim \mathcal{N} \left(\begin{bmatrix} \boldsymbol{\mu}_1 - \boldsymbol{\mu}_2 \\ \Phi \left(\frac{\boldsymbol{\mu}_1 - \boldsymbol{\mu}_2}{\sqrt{2}\sigma} \right) \end{bmatrix}, \frac{1}{N} \begin{bmatrix} 2\sigma^2 & \sqrt{2}\sigma\phi(a) \\ \sqrt{2}\sigma\phi(a) & \phi(a) - \phi^2(a) \end{bmatrix} \right).$$

Define the standardized variables

$$\begin{bmatrix} X \\ Y \end{bmatrix} := \begin{bmatrix} \frac{\frac{1}{N} \sum_{i=1}^N (z_1^{(i)} - z_2^{(i)}) - (\boldsymbol{\mu}_1 - \boldsymbol{\mu}_2)}{\sqrt{2}\sigma/\sqrt{N}} \\ \frac{\frac{1}{N} \sum_{i=1}^N \mathbb{1}_{z_1^{(i)} > z_2^{(i)}} - \phi(a)}{\sqrt{\phi(a) - \phi^2(a)}/\sqrt{N}} \end{bmatrix},$$

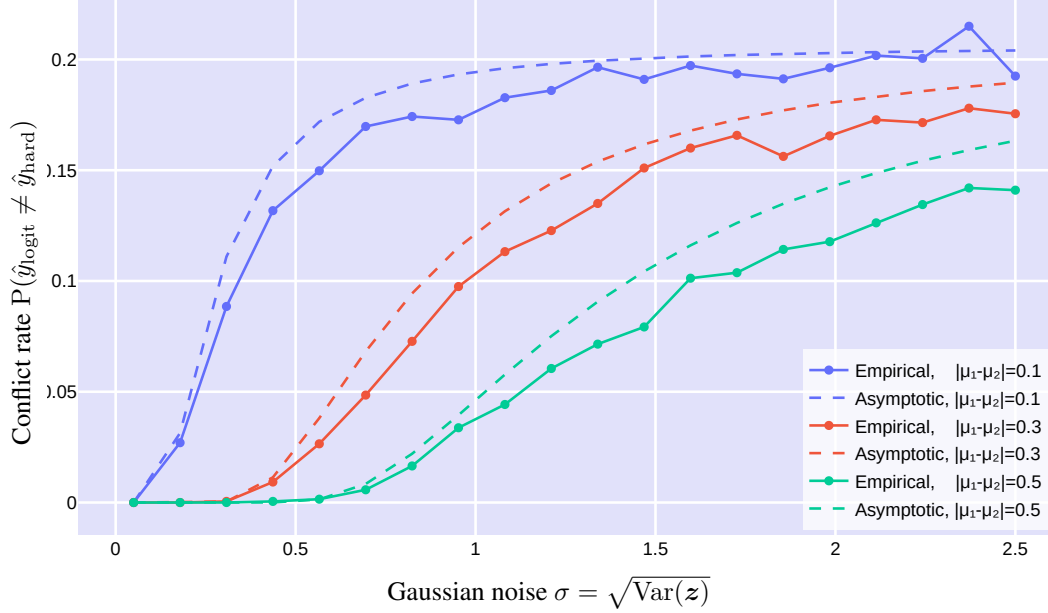


Figure 5: **Monte Carlo simulation.** The conflict probability increases as $\text{Var}(z)$ grows. In this simulation, we consider distributions: $\{z \sim \mathcal{N}(\mu, \sigma I) \mid \mu \in \{(1, 0.9), (1, 0.7), (1, 0.5)\}, \sigma \in [0.05, 0.25]\}$. The solid curves show Monte Carlo estimates of the relationship between σ and $P(\hat{y}_{\text{logit}} \neq \hat{y}_{\text{hard}})$, while the dashed curves correspond to the theoretical (asymptotic) predictions. The empirical and theoretical results are closely matched.

which jointly follow

$$\begin{bmatrix} X \\ Y \end{bmatrix} \sim \mathcal{N} \left(\begin{bmatrix} 0 \\ 0 \end{bmatrix}, \begin{bmatrix} 1 & \sqrt{\frac{N\phi(a)}{1-\phi(a)}} \\ \sqrt{\frac{N\phi(a)}{1-\phi(a)}} & 1 \end{bmatrix} \right).$$

We now compute the probability of conflict between the logit-averaging and the hard voting method. First,

$$\begin{aligned} P(\hat{y}_{\text{logit}} = 1, \hat{y}_{\text{hard}} = 2) &= P \left(\frac{1}{N} \sum_{k=1}^N (z_1^{(k)} - z_2^{(k)}) > 0, \frac{1}{N} \sum_{i=1}^N \mathbb{1}_{z_1^{(k)} > z_2^{(k)}} \leq \frac{1}{2} \right) \\ &= P \left(X > -\sqrt{N}a, Y \leq \frac{(1/2 - \phi(a))\sqrt{N}}{\sqrt{\phi(a) - \phi^2(a)}} \right) \\ &= \Phi \left(\frac{(1/2 - \phi(a))\sqrt{N}}{\sqrt{\phi(a) - \phi^2(a)}} \right) \\ &\quad - \Phi_2 \left(-a\sqrt{N}, \frac{(1/2 - \phi(a))\sqrt{N}}{\sqrt{\phi(a) - \phi^2(a)}}; \frac{\phi(a)}{\sqrt{\Phi(a) - \Phi^2(a)}} \right). \end{aligned} \quad (5)$$

Similarly,

$$\begin{aligned}
P(\hat{y}_{\text{logit}} = 2, \hat{y}_{\text{hard}} = 1) &= P\left(\frac{1}{N} \sum_{k=1}^N (z_1^{(k)} - z_2^{(k)}) \leq 0, \frac{1}{N} \sum_{i=1}^N \mathbb{1}_{z_1^{(k)} > z_2^{(k)}} > \frac{1}{2}\right) \\
&= P\left(X \leq -\sqrt{N}a, Y > \frac{(1/2 - \phi(a))\sqrt{N}}{\sqrt{\phi(a) - \phi^2(a)}}\right) \\
&= \Phi(-\sqrt{N}a) \\
&\quad - \Phi_2\left(-a\sqrt{N}, \frac{(1/2 - \phi(a))\sqrt{N}}{\sqrt{\phi(a) - \phi^2(a)}}; \frac{\phi(a)}{\sqrt{\Phi(a) - \Phi^2(a)}}\right). \tag{6}
\end{aligned}$$

Therefore, the total conflict probability is

$$\begin{aligned}
P(\hat{y}_{\text{logit}} \neq \hat{y}_{\text{hard}}) &= P(\hat{y}_{\text{logit}} = 1, \hat{y}_{\text{hard}} = 2) + P(\hat{y}_{\text{logit}} = 2, \hat{y}_{\text{hard}} = 1) \\
&= \Phi(-\sqrt{N}a) + \Phi\left(\frac{(1/2 - \phi(a))\sqrt{N}}{\sqrt{\phi(a) - \phi^2(a)}}\right) \\
&\quad - 2\Phi_2\left(-a\sqrt{N}, \frac{(1/2 - \phi(a))\sqrt{N}}{\sqrt{\phi(a) - \phi^2(a)}}; \frac{\phi(a)}{\sqrt{\Phi(a) - \Phi^2(a)}}\right). \tag{7}
\end{aligned}$$

This expression indicates that the conflict rate increases as $\text{Var}(z) = \sigma^2$ grows. Fig. 5 provides empirical support for this conclusion. The solid curves represent Monte Carlo estimates of the relationship between σ and $P(\hat{y}_{\text{logit}} \neq \hat{y}_{\text{hard}})$, while the dashed curves correspond to the theoretical (asymptotic) predictions. We observe that the empirical and theoretical curves exhibit consistent trends, with closely matching derivatives.

B Hölder Condition

Figure 6 provides an intuitive visualization of how different data augmentation strategies influence the variance of logits under the Hölder continuity assumption. According to Eq. (1), the distance between logit vectors is bounded by the distance between augmented inputs. As illustrated in the left example, translation preserves the semantic structure of the image but introduces large pixel-wise differences between augmented samples, leading to a larger input distance $\|\psi_i(\mathbf{x}) - \psi_j(\mathbf{x})\|$ and consequently higher variance in the resulting logits. In contrast, the right example shows random erasing, which applies stronger noise but gives smaller overall pixel-wise differences across augmentations. This reduces the variance of the logit vector, producing more concentrated predictions that are better suited for stable aggregation. The figure thus highlights that not all augmentations contribute equally to logit stability.

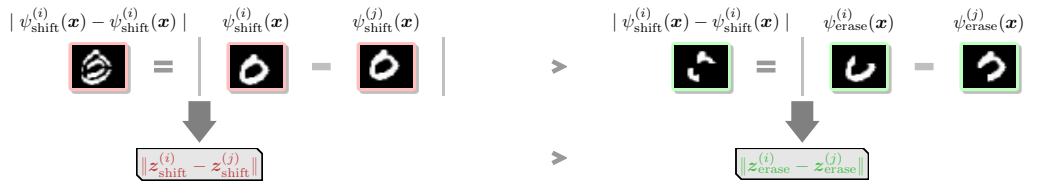


Figure 6: **Varying Effects of Data Augmentation Methods on the Variance of Logits.** Under Hölder continuity, larger changes in the input lead to larger changes in the logits. **Left:** Translation preserves the semantic content of the image but introduces large pixel-wise differences, resulting in a higher variance in the logit distribution. **Right:** Random erasing applies stronger modifications to the image, but the overall pixel-wise differences are smaller, leading to more concentrated logits that are better suited to stable aggregation.

Table 2: Ablation study of StableTTA versus standard TTA under varying numbers of experts (N) across multiple architectures. StableTTA consistently outperforms TTA under MixUp and CutMix data augmentations.

Weight	Params	N	Acc@1	Acc@5
AlexNet	61.1M	4	65.590	87.022
AlexNet	61.1M	8	68.604	89.432
AlexNet	61.1M	16	70.496	90.510
AlexNet	61.1M	32	71.258	90.938
ResNet50 [†]	25.6M	4	88.556	98.858
ResNet50 [†]	25.6M	8	89.542	99.098
ResNet50 [†]	25.6M	16	90.232	99.172
ResNet50 [†]	25.6M	32	90.612	99.240
ViT_B_16	86.6M	4	87.052	98.470
ViT_B_16	86.6M	8	88.206	98.938
ViT_B_16	86.6M	16	89.048	99.030
ViT_B_16	86.6M	32	89.382	99.074

Table 3: Sensitivity analysis of StableTTA over K and N . Results show robustness to K , consistent gains with larger N , and significant drops when logit processing is disabled ($K = C$).

Model	K	N = 4		N = 8		N = 16		N = 32	
		Acc@1	Acc@5	Acc@1	Acc@5	Acc@1	Acc@5	Acc@1	Acc@5
AlexNet (61.1M) (0.71GFLOPS)	1	78.412	93.182	84.638	96.134	87.942	97.530	89.576	98.052
	2	78.444	93.262	84.982	96.312	87.946	97.528	89.496	98.052
	5	78.804	93.328	84.666	96.220	87.984	97.412	89.484	98.108
	10	78.750	93.434	84.810	96.216	87.864	97.470	89.532	98.030
	20	78.540	93.320	84.778	96.160	88.072	97.540	89.530	98.076
	C	66.212	83.420	71.606	91.158	74.948	94.520	76.918	96.222
ResNet50 [†] (25.6M) (4.09GFLOPS)	1	91.524	99.082	93.788	99.614	95.076	99.802	95.706	99.860
	2	91.436	99.120	93.830	99.624	95.022	99.780	95.552	99.834
	5	91.484	99.084	93.746	99.622	94.998	99.818	95.656	99.860
	10	91.276	99.108	93.878	99.676	95.192	99.800	95.646	99.852
	20	91.576	99.126	93.726	99.598	95.008	99.770	95.642	99.876
	C	86.670	96.534	89.820	98.822	92.034	99.542	93.110	99.744
ViT_B_16 (86.6M) (17.56GFLOPS)	1	91.488	99.142	93.906	99.676	95.308	99.822	95.822	99.864
	2	91.604	99.128	94.000	99.670	95.304	99.810	95.826	99.878
	5	91.602	99.112	93.894	99.682	95.088	99.820	95.824	99.884
	10	91.668	99.152	94.042	99.656	95.114	99.820	95.852	99.888
	20	91.468	99.126	94.972	99.648	95.234	99.816	95.940	99.904
	C	86.710	96.578	89.898	98.844	91.648	99.540	92.832	99.744

C Ablation Study

Table 2 reports the performance comparison between standard TTA and our StableTTA under MixUp and CutMix augmentation strategies, across different architectures and varying numbers of experts (N). Consistent with the trends observed in Fig. 4a, StableTTA outperforms TTA. Increasing N steadily improves both top-1 and top-5 accuracy for all models, including AlexNet, ResNet50, and ViT-B16. However, the performance gains gradually diminish as N increases, indicating a clear saturation effect. This table provides evidence emphasizing the advantages of StableTTA.

D Sensitivity Analysis

Table 3 presents a detailed sensitivity analysis of StableTTA with respect to the number of candidates K and experts N across different architectures. Consistent with the trends observed in Fig. 4b, StableTTA exhibits strong robustness to the choice of K , with performance remaining largely stable across a wide range of values. Increasing N consistently improves both top-1 and top-5 accuracy, while the impact of varying K is relatively minor. Notably, when logit processing is disabled ($K = C$), performance drops significantly across all models, reaffirming the critical role of our logit processing (NSS) in achieving accuracy gains. Overall, these results demonstrate that StableTTA delivers stable, reliable improvements without requiring careful hyperparameter tuning.